

Unsupervised Anomaly Detection with Multi-scale Interpolated Gaussian Descriptors

Yuanhong Chen^{1*} Yu Tian^{1,2*†} Guansong Pang¹ Gustavo Carneiro¹
¹ Australian Institute for Machine Learning, University of Adelaide
² South Australian Health and Medical Research Institute

Abstract

Current unsupervised anomaly detection and pixel-wise anomaly localisation systems are commonly formulated as one-class classifiers that depend on an effective estimation of the distribution of normal images and robust criteria to identify anomalies. However, the distribution of normal images estimated by current systems tends to be unstable for classes of normal images that are under-represented in the training set, and the anomaly identification criteria commonly explored in the field does not work well for multi-scale structural and non-structural anomalies. In this paper, we introduce a new unsupervised anomaly detection and localisation method designed to address these two issues. More specifically, we introduce a normal image distribution estimation method that is robust to under-represented classes of normal images – this method is based on adversarially interpolated descriptors from training images and a Gaussian classifier. We also propose a new anomaly identification criterion that can accurately detect and localise multi-scale structural and non-structural anomalies. In extensive experiments on MNIST, Fashion MNIST, CIFAR10, MVTec AD and two medical datasets, our approach shows better results than the current state of the art in the standard experimental setup for unsupervised anomaly detection and localisation. Code is available at <https://github.com/tianyu0207/IGD>.

1. Introduction

Anomaly detection and pixel-wise anomaly localisation are critical tasks in the identification of defects on industry objects [7] or abnormalities from medical images [65, 66, 74, 76]. Given that most of the training sets available for this task only contain normal images, methods are usually formulated as one-class classifiers (OCC) [27, 29, 41, 45, 56–58, 62, 78, 89] – these methods are commonly re-

*First two authors contributed equally to this work.

†Corresponding author.

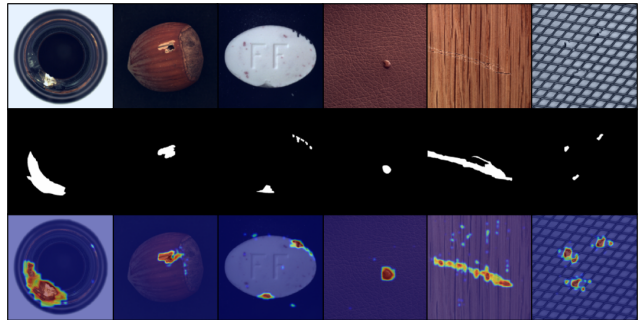


Figure 1. Qualitative results of our anomaly localisation results on the MVTec AD dataset (red = high probability of anomaly). Top, middle and bottom rows show the testing images, ground-truth masks and predicted heatmaps, respectively.

ferred to as unsupervised anomaly detectors (UAD). OCCs aim to first estimate the distribution of normal images in the training set and then use a criterion (e.g., distance to the one-class centre [62]) to detect and localise anomalies in test images. Hence, the **functionality of OCCs** depends on the **normal image distribution generalisation** and on the **anomaly identification criteria**.

When the estimated distribution of normal images [23, 54, 62] does not generalise well, it does not fit under-represented types of normal images from the training set, resulting in false detection of anomalies. Methods to constrain the distribution of normal images to lie at specific regions of the feature space can mitigate this issue [54, 62], but they still do not provide a robust generalisation, as evidenced by their results. A recent trend in the field to address this generalisation issue is based on self-supervision [6, 22], which has been successful in synthetic anomaly detection problems, such as CIFAR10 [34]. However, self-supervision alone shows poor generalisation for anomaly detection in real-world data sets [6, 22], such as MVTec AD [7]. Moreover, there is no evidence that self-supervised approaches can work well for unsupervised anomaly localisation. Therefore, although promising, it is unclear if self-supervision alone will be enough to produce competitive

real-world anomaly localisation results.

The criteria to detect and localise image anomalies are usually based on the reconstruction loss between the original image and its reconstructed image obtained from a generative model fitted to represent the normal training data [23, 31, 41, 49, 50, 60, 63, 64, 86]. Such reconstruction loss generally relies on the mean square error (MSE), which can miss multi-scale structural anomalies [51, 81]. Recently, a method based on structural similarity index measure (SSIM) [81] has been proposed [9] to detect single-scale structural anomalies, but anomalies can exhibit abnormality in varying scales. Therefore, it is important that the criteria to identify anomalies take into account global and local reconstruction errors, with the local errors considering multi-scale structural and non-structural anomalies.

In this paper, we introduce a novel unsupervised anomaly detection and localisation method that tackles the two issues described above. **To address the normal image distribution generalisation**, we propose the **interpolated Gaussian descriptor (IGD)**. Our IGD consists of a new Gaussian Support Vector Data Descriptor (GSVDD) model, which enables a robust estimation of the normal image distribution, driven by the adversarially constrained auto-encoder interpolation (ACAI) [10] that increases sample density of the training set in the latent space without adding more data in the training set. **The improvement of the anomaly detection criteria** is based on a **new combination of multi-scale structural similarity index measure (MS-SSIM) [81, 82, 90] and mean absolute error (MAE)** to accurately identify structural and non-structural anomalies of varying sizes. The **training** of our model **minimises a combined classification and reconstruction losses**, which is **new in anomaly detection**, to the best of our knowledge.

We evaluate our framework on MNIST [36], Fashion MNIST (FMNIST) [85] CIFAR10 [34], MVTec AD [7], a medical Hyper-Kvasir (colonoscopy) [12] and LAG (glaucoma) [37] datasets. Our method shows the best results on all six datasets including synthetic anomaly detection problems, industrial defect detection and localisation, and malignant lesion detection. This indicates that our approach can generalise well across different application domains.

2. Related Work

2.1. Unsupervised Anomaly Detection

Unsupervised anomaly detection (UAD) is generally solved with OCCs [68] that clusters the features extracted from normal training images around a particular region of the feature space, and classification is based on how close test image features are from this region. Initially, OCCs were explored with hand-crafted features [4, 48, 80, 88], but more recently, end-to-end deep learning models learn both the feature extractor and classifier together [1, 6, 8, 15, 18, 22,

46, 49, 52, 52, 54, 62, 79, 93]. A representative model of these approaches is SVDD [73], which forces normal image features to be inside a hyper-sphere with a pre-defined centre and a radius that is minimised to contain all training images. Then, test images that fall inside the learned hyper-sphere are classified as normal, and the ones outside are anomalous. Although powerful, the hard boundary of SVDD can cause the model to overfit the training data – this problem was tackled by Ruff et al. [62] with a soft-boundary SVDD, but it still can overfit given that it does not optimise for other latent variables (e.g., hyper-sphere centre).

Other UAD methods rely on generative models. In [54], a generative adversarial network (GAN) is trained to produce normal samples, and its discriminator is used to detect anomalies, but the hard training process of GANs represents a disadvantage of this approach. Auto-encoders (AE) [13, 23, 31, 41, 50, 60, 63, 64, 78, 86, 94] are trained to reconstruct normal data, and the anomaly score is defined as the reconstruction error between the input and reconstructed images. AE approaches depend on the MSE reconstruction loss, which does not work well for structural anomalies. Alternatively, single-scale SSIM loss [9] tends to work poorly for non-structural anomalies and structural anomalies of sizes outside that single scale.

The robustness of anomaly detectors can be improved if they are fine-tuned from models pre-trained on other tasks, such as image classification [6, 78], video understanding [71, 75, 84, 91], and object detection [31]. Venkataraman et al. [78] utilise a model pre-trained on ImageNet [20] and CelebA [44] that shows promising results on several anomaly detection benchmarks. The state-of-the-art (SOTA) model by Bergmann et al. [8] uses a student-teacher framework to predict anomalies with multiple shallow students to regress the output of a teacher network, which is pre-trained on ImageNet. Recent works [6, 22] use self-supervised training to increase the effectiveness of the learned embeddings. For instance, GeoTrans [22] trains a classifier to predict the geometric transformation applied to normal training data, and combines the prediction of each type of transformation as the anomaly score for transformed testing images. Bergman et al. [6] extend SVDD [62] to construct a hyper-sphere for each type of data augmentation. During testing, they predict the probability that all transformed samples fall into their respective hyper-spheres. From the evidence above, self-supervised learning is effective only in data sets where the anomaly is represented by the whole image (e.g., a dog image is an anomaly for a system trained with “normal” cat images), such as CIFAR10. Given the positive results by [8, 22], we also rely on pre-training.

2.2. Unsupervised Anomaly Localisation

Unsupervised anomaly localisation targets the segmentation of anomalous image pixels or patches, containing,

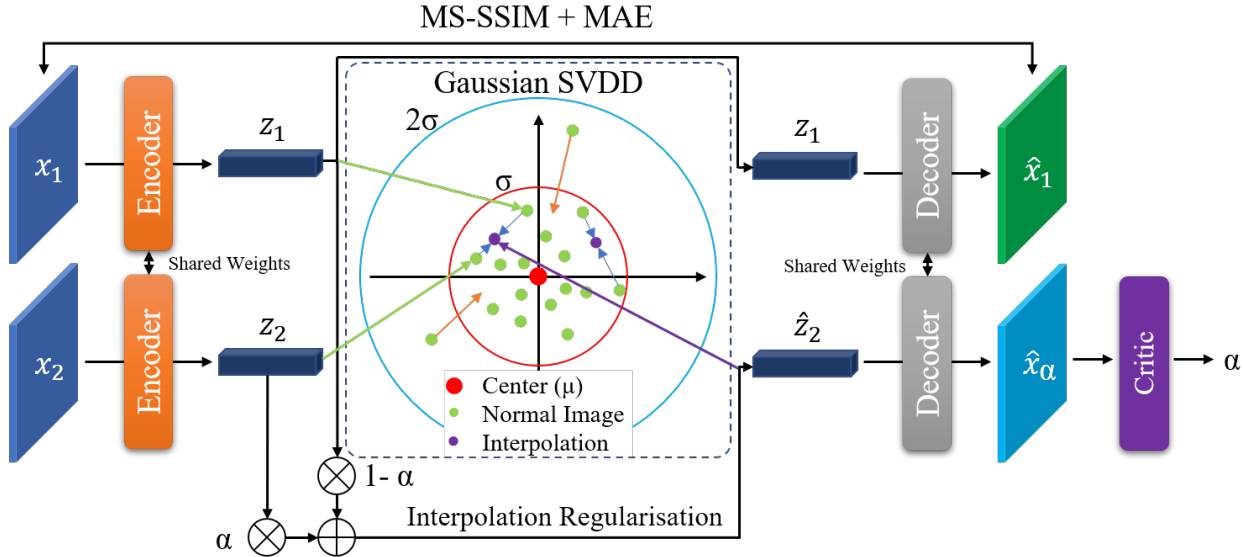


Figure 2. Our method introduces: 1) the Gaussian SVDD classifier trained to map normal images to the mean of a Gaussian distribution, trained with samples from images and interpolated features that are also used to train a critic network to uncover the mixing up coefficient α ; 2) a combination of a MS-SSIM and MAE reconstruction losses to enable the detection of multi-scale structural and non-structural anomalies; and 3) a learning based on a combined classification (GSVDD) and reconstruction (MS-SSIM+MAE) losses.

for example, lesions from medical images [38, 43], or defects in industry images [7, 8]. The main idea explored is based on extending the image based OCC to a pixel-based OCC. Then, testing produces a pixel-wise anomaly score map, where a pixel with a high score represents an anomalous pixel [2, 5, 9, 59, 66]. The way such scores are computed are based on the same anomaly detection criteria presented above in Sec. 2.1. In general, methods that can localise anomalies [8, 65, 78] are tuned to particular anomaly sizes and structure, which can cause then to miss anomalies outside that range of sizes and structure.

3. Method

In this section, we introduce our **main contributions**, namely: 1) the **Interpolated Gaussian Descriptor (IGD)** that combines the adversarially constrained auto-encoder interpolation (ACAI) [10] and an extension for the SVDD model [73] to work with a Gaussian classifier trained with the EM algorithm [19]; 2) the **combination of MS-SSIM and MAE** as criteria to identify structural and non-structural anomalies of varying sizes; and 3) the learning based on a **combined classification and reconstruction losses**.

We assume the availability of a training set that contains only normal samples and is denoted by $\mathcal{D} = \{\mathbf{x}_i\}_{i=1}^{|\mathcal{D}|}$, where $\mathbf{x} \in \mathcal{X} \subset \mathbb{R}^{W \times H \times 3}$ represents an RGB image of width W and height H . The testing set contains normal and anomalous images, where anomalous images have segmen-

tation map annotations. This testing set is defined by $\mathcal{T} = \{(\mathbf{x}_i, y_i, \mathbf{b}_i^{(y_i)})\}_{i=1}^{|\mathcal{T}|}$, where $y_i \in \mathcal{Y} = \{\text{normal, anomalous}\}$, the segmentation map with the anomaly is denoted by $\mathbf{b}_i^{(y_i)} \in \{0, 1\}^{W \times H}$ (0 denotes a normal and 1 denotes an anomalous pixel in the image \mathbf{x}_i) if $y_i = \text{anomalous}$, and $\mathbf{b}_i^{(y_i)} = 0^{W \times H}$ if $y_i = \text{normal}$.

The model is trained with the following loss (see Fig. 2):

$$\frac{1}{|\mathcal{D}|} \sum_{i=1}^{|\mathcal{D}|} \ell_h(\mathbf{x}_i) + \ell_d(\mathbf{x}_i) + \ell_{f,g}(\mathbf{x}_i), \quad (1)$$

where $\ell_h(\cdot)$ is the loss for training the **GSVDD classifier**, $\ell_d(\cdot)$ is for ACAI's **interpolation model**, and $\ell_{f,g}(\cdot)$ for the **auto-encoder model** based on the MS-SSIM and MAE reconstruction losses. The loss in (1), which we explain in more detail in Sections 3.1 and 3.2, is used to train two models: the global one works on the whole image \mathbf{x} , and the local model works on image patches $\mathbf{x}^{(L)}(\omega) \in \mathcal{X}^{(L)} \subset \mathbb{R}^{W^{(L)} \times H^{(L)} \times 3}$, with $W^{(L)} < W$ and $H^{(L)} < H$, centred at pixel $\omega \in \Omega$ (Ω is the image lattice). During inference, the results from the global and local models are combined to produce multi-scale anomaly detection and localisation. Hence, the combination of the two models enables a multi-scale analysis of the image.

3.1. Interpolated Gaussian Descriptor (IGD)

Our proposed IGD model consists of the auto-encoder to reconstruct the input image, and the interpolated GSVDD

classifier to constrain the latent space of the auto-encoder (See Fig. 2).

GSVDD Classifier: The GSVDD constrains the latent space of the auto-encoder with the following loss:

$$\ell_h(\mathbf{x}) = h_\gamma(f_\theta(\mathbf{x})), \quad (2)$$

where the GSVDD classifier is defined with $h_\gamma(f_\theta(\mathbf{x})) = 1 - \exp\left(-\frac{\|f_\theta(\mathbf{x}) - \mu_\gamma\|_2^2}{\sigma_\gamma^2}\right)$, $f_\theta : \mathcal{X} \rightarrow \mathcal{Z}$ represents the encoder parameterised by θ , with $\mathcal{Z} \subset \mathbb{R}^Z$ denoting the space of latent embeddings of the auto-encoder. The mean and standard deviation values above are estimated with $\mu_\gamma = \frac{1}{|\mathcal{D}|} \sum_{i=1}^{|\mathcal{D}|} f_\theta(\mathbf{x}_i)$ and $\sigma_\gamma^2 = \frac{\kappa}{|\mathcal{D}|} \sum_{i=1}^{|\mathcal{D}|} \|f_\theta(\mathbf{x}_i) - \mu_\gamma\|_2^2$, where $\kappa \in (0, 1]$ is a constant that regularises the estimation of σ_γ^2 to prevent numerical instabilities during training. Our GSVDD replaces the hyper-sphere used in deep SVDD (DSVDD) [62] by a Gaussian, and treats the Gaussian mean and covariance as latent variables to be estimated during the expectation stage of the EM optimisation [19]. Such optimisation has the potential to be less sensitive to outliers compared with the one proposed for DSVDD [62], which explicitly minimises the radius of the hyper-sphere representing the normal embeddings, but fixes the centre of this hyper-sphere at the first epoch.

Interpolation model: To facilitate and regularise the GSVDD training, we linearly interpolate the latent embeddings from different input images, and estimate the interpolation coefficient with the **critic network** [10]. The intuition behind this interpolation model is to make the distribution of training normal samples denser in the latent embedding space, reducing the likelihood that anomaly embeddings may sit in the same region of the embedding space occupied by normal samples. Unlike Mix-up [87], our interpolation model, based on ACAI [10], is a self-supervised method that does not rely on data augmentation on the input space and does not interpolate training labels, making it more adequate for our problem because it enforces a compact and dense distribution of normal samples to be estimated for the GSVDD classifier. The critic network is represented by

$$\hat{\alpha} = d_\psi(\hat{\mathbf{x}}_\alpha), \quad (3)$$

where $\hat{\mathbf{x}}_\alpha = g_\phi(\alpha \mathbf{z}_1 + (1 - \alpha) \mathbf{z}_2)$ represents the reconstruction of the interpolation of $\mathbf{z}_1 = f_\theta(\mathbf{x}_1)$ and $\mathbf{z}_2 = f_\theta(\mathbf{x}_2)$ (with $\alpha \sim \mathcal{U}(0, 0.5)$, $\mathbf{x}_1, \mathbf{x}_2 \in \mathcal{D}$, $\mathbf{x}_1 \neq \mathbf{x}_2$, and \mathcal{U} denoting a uniform distribution) [10], and $g_\phi : \mathcal{Z} \rightarrow \mathcal{X}$ denotes the decoder of the auto-encoder model. The goal of the critic network $d_\psi(\cdot)$ is to predict the interpolation coefficient α . The critic network in (3) is similar to the discriminator in GAN [24], and relies on the following adversarial loss to be optimised [10]

$$\ell_d(\mathbf{x}) = \|d_\psi(\hat{\mathbf{x}}_\alpha) - \alpha\|_2^2 + \|d_\psi(\hat{\mathbf{x}}_\zeta)\|_2^2, \quad (4)$$

where $\hat{\mathbf{x}}_\alpha$ is defined in (3), and $\hat{\mathbf{x}}_\zeta = \zeta \mathbf{x} + (1 - \zeta) \hat{\mathbf{x}}$, with $\zeta \sim \mathcal{U}(0, 1)$ and $\hat{\mathbf{x}}$ denoting a reconstruction of \mathbf{x} by the auto-encoder. The first term of this loss minimises the critic’s prediction error for α and the second term regularises the training to ensure that the critic predicts $\hat{\alpha} = 0$ when the original image is interpolated with its own reconstruction in the image space \mathcal{X} .

Auto-encoder model: The optimisation of the encoder and decoder models minimises the following loss

$$\ell_{f,g}(\mathbf{x}) = \ell_r(\mathbf{x}, \hat{\mathbf{x}}) + \lambda \|d_\psi(\hat{\mathbf{x}}_\alpha)\|_2^2, \quad (5)$$

where $\hat{\mathbf{x}}$ is a reconstruction of \mathbf{x} by the auto-encoder, with the image reconstruction loss $\ell_r(\cdot)$ based on a combined MS-SSIM and MAE reconstruction losses (to be defined below in (6)), and λ is a hyperparameter to weight the regularisation term. This regularisation fools the critic to output $\hat{\alpha} = 0$ for interpolated embeddings, independently of α , following standard adversarial training [24].

3.2. Detecting Structural and Non-structural Anomalies

The combination of MS-SSIM and MAE losses to detect structural and non-structural anomalies of varying sizes is another contribution of our paper – see Fig. 3. Mean square error (MSE) has been used in anomaly detection [23, 31, 60, 78, 86] and it has been shown to be effective to detect non-structural anomalies, caused by global changes in the image. However, MSE tends to be too brittle and produce high values when there are small (but global) localisation errors and it also fails to detect structural anomalies, represented by image abnormalities that have strong inter-dependencies between neighbouring pixels. Also, the MSE loss can overfit to large reconstruction errors, which is commonly solved by replacing it with mean absolute error (MAE), which although more robust to overfitting, still has the same issues as MSE. That motivated the use of SSIM [81] in anomaly detection [9], but SSIM may fail to detect non-structural anomalies. Furthermore, previous methods do not explore multi-scale reconstruction losses, which is particularly important for structural anomalies of varying sizes. Therefore, we propose to combine the multi-scale SSIM (MS-SSIM) [82] with MAE to enable the detection of structural and non-structural multi-scale anomalies.

The combined MAE and MS-SSIM reconstruction losses, denoted by ℓ_r in (5), is defined as:

$$\ell_r(\mathbf{x}, \hat{\mathbf{x}}) = \sum_{\omega \in \Omega} \rho |\mathbf{x}(\omega) - \hat{\mathbf{x}}(\omega)| + (1 - \rho) \left(1 - m(\mathbf{x}(\omega), \hat{\mathbf{x}}(\omega))\right), \quad (6)$$

where $\rho \in [0, 1]$, $m(\mathbf{x}(\omega), \hat{\mathbf{x}}(\omega)) \in [0, 1]$ denotes the MS-SSIM score [82], with larger values indicating higher similarity between patches $\omega \in \Omega$ of the

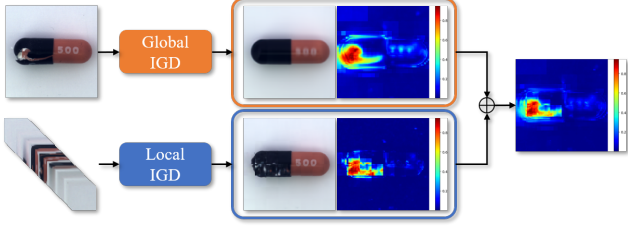


Figure 3. Example of the multi-scale structural and non-structural anomaly localisation result for an MVTec AD [7] image, using both the local and global IGD models use the anomaly local score $l(\mathbf{x}(\omega))$ in (10). The global model tends to produce smooth results but with some mistakes, while the local model produces jagged results, but without the global mistakes, so by combining the two results, we obtain a smooth and correct anomaly heatmap.

original and reconstructed images. Definitions of the global and local MS-SSIM scores, $m^{(G)}(\mathbf{x}(\omega), \hat{\mathbf{x}}(\omega))$ and $m^{(L)}(\mathbf{x}^{(L)}(\omega), \hat{\mathbf{x}}^{(L)}(\omega))$, respectively, for the global (using the whole image) and local (using image patches) IGD models are demonstrated in Fig. 3. Note that our global and local IGD models use the same network architecture, but are trained separately using the combined MS-SSIM and MAE reconstruction loss (6), in addition to the other loss terms in (1).

3.3. Training and Inference of the Global and Local IGD

To enable a fair comparison between our method and previous approaches in the field [6, 8, 22, 78], we pre-train the encoders for the global and local IGD models either with self-supervised learning (SSL) [14] or knowledge distillation (KD) [8, 25, 30]. We try both pre-training approaches because they have been shown to produce encoders that can fit more easily different types of downstream tasks. For self-supervision pre-training, we follow the contrastive learning of visual representations using several types of data augmentation [14] with the images from \mathcal{D} . For KD, we pre-train the encoder $f_\theta(\mathbf{x})$ to reconstruct the embeddings of the images in \mathcal{D} produced by an ImageNet pre-trained model.

After pre-training, we train the global and local IGD models separately, following an EM optimisation. The E-step estimates the values of the latent variables μ_γ and σ_γ in (2). For the M-step, we minimise the loss in (1) by optimising θ with respect to $\ell_{f,g}(\cdot)$ in (5) and $\ell_h(\cdot)$ in (2), ϕ with respect to $\ell_{f,g}(\cdot)$ in (5), and ψ with respect to $\ell_d(\cdot)$ in (4).

During inference, **anomaly detection** is performed by combining the global and local IGD anomaly scores for a testing image \mathbf{x} as in:

$$s(\mathbf{x}) = s^{(G)}(\mathbf{x}) + s^{(L)}(\mathbf{x}). \quad (7)$$

The global score in (7) is defined as

$$s^{(G)}(\mathbf{x}) = \ell_r^{(G)}(\mathbf{x}, \hat{\mathbf{x}}) + \ell_h^{(G)}(\mathbf{x}), \quad (8)$$

where $\ell_r^{(G)}(\cdot)$ denotes the reconstruction loss from (6) and $\ell_h^{(G)}(\cdot)$ denotes the GSVDD loss from (2) (both computed with the global IGD model using the whole images), and $\hat{\mathbf{x}}$ is the reconstruction of \mathbf{x} produced by the auto-encoder. The local score in (7) is defined as

$$s^{(L)}(\mathbf{x}) = \max_{\omega \in \Omega} \left(\ell_r^{(L)}(\mathbf{x}^{(L)}(\omega), \hat{\mathbf{x}}^{(L)}(\omega)) + \ell_h^{(L)}(\mathbf{x}^{(L)}(\omega)) \right), \quad (9)$$

where $\ell_r^{(L)}(\cdot)$ and $\ell_h^{(L)}(\cdot)$ are the reconstruction and GSVDD losses computed from the local model, with $\mathbf{x}^{(L)}(\omega)$ denoting an image patch of size $W^{(L)} \times H^{(L)} \times 3$ at pixel $\omega \in \Omega$. The use of max pooling of the local scores in (9) facilitates detection of images that contain anomalies covering a small region of the image. **Anomaly localisation** is computed for each pixel $\omega \in \Omega$ to produce a local score with

$$l(\mathbf{x}(\omega)) = \ell_r^{(G)}(\mathbf{x}(\omega), \hat{\mathbf{x}}(\omega)) + \ell_r^{(L)}(\mathbf{x}^{(L)}(\omega), \hat{\mathbf{x}}^{(L)}(\omega)). \quad (10)$$

In (10), we have

$$\ell_r^{(G)}(\mathbf{x}(\omega), \hat{\mathbf{x}}(\omega)) = \rho |\mathbf{x}(\omega) - \hat{\mathbf{x}}(\omega)| + (1 - \rho) \left(1 - m^{(G)}(\mathbf{x}(\omega), \hat{\mathbf{x}}(\omega)) \right), \quad (11)$$

where ρ and $m^{(G)}(\cdot)$ are defined in (6) and $\hat{\mathbf{x}}$ is a reconstruction of \mathbf{x} produced by the global IGD model. The $\ell_r^{(L)}(\mathbf{x}^{(L)}(\omega), \hat{\mathbf{x}}^{(L)}(\omega))$ in (10) is similarly defined using the local IGD model. Thus, the anomaly localisation final map is a heatmap with high values representing regions that are likely to contain anomalies, as displayed in Fig. 3.

4. Experiments

4.1. Datasets and Evaluation Metric

Datasets: We use six different datasets to evaluate our methods, namely MNIST [36], Fashion MNIST [85], CIFAR10 [34] and MVTec AD [7], Hyper-Kvasir [12] and LAG [37]. MNIST, Fashion MNIST and CIFAR10 have been widely used as benchmarks for image anomaly detection, and we follow the same experimental protocol as described in [1, 8, 16, 23, 54, 62, 78]. CIFAR10 contains 60,000 images with 10 classes. MNIST and Fashion MNIST contains 70,000 images with 10 classes of handwritten digits and fashion products, respectively.

MVTEC AD [7] is a recently released data set that contains 5,354 high-resolution real-world images of 15 different industry object and textures. The normal class of

MVTec AD is formed by the images without defects and consists of 3,629 images for training and 467 images for testing. The anomalous class has more than 70 categories of defects (such as dents, structural fails, contamination, etc.) and contains 1,258 images. Furthermore, MVTec AD also provides pixel-wise ground truth annotations for all anomalies, allowing the evaluation of anomaly detection and localisation.

We also tested our method on two publicly available medical datasets: Hyper-Kvasir [12] and LAG [37] for polyp and glaucoma detection, respectively. For Hyper-Kvasir, we have 1,600 normal images without polyps in the training set and 500 in the testing set; and 1,000 abnormal images containing polyps in the testing set. For LAG, we have 2,343 normal images without glaucoma in the training set; and 800 normal images and 1,711 abnormal images with glaucoma for testing.

Evaluation Metric: For *anomaly detection*, we use area under the receiver operating characteristic curve (AUC) for all data sets [1, 8, 16, 23, 54, 62, 78]. On MNIST, Fashion MNIST and CIFAR10, we use the same protocol as [1, 6, 8, 22, 54, 62, 78], where training uses a single class as the normal data, with the nine remaining classes denoting the anomalous data, and inference relies on a non-augmented test image. We report the mean AUC over the 10 classes for the above three data sets. On MVTec AD, as suggested in [8, 78], we evaluate anomaly detection performance not only with AUC, but also with mean accuracy. For the colonoscopy and glaucoma detection datasets, we evaluate the methods using AUC. For *anomaly localisation*, we follow [78] and compute the mean pixel-level AUC between the generated heatmap and the ground truth segmentation map for each anomalous image in the testing set on MVTec AD.

4.2. Implementation Details

We implement our framework using Pytorch [53]. The model was trained with Adam optimiser [32] using a learning rate of 0.0001, weight decay of 10^{-6} , batch size of 64 images, 128 epochs for MNIST, Fashion MNIST and CIFAR 10, and 256 epochs for MVTec AD, Hyper-Kvasir and LAG. We defined the latent space to have $Z = 128$ dimensions in (2). Following [21, 90], we set $\rho = 0.15$ to balance the contribution of MAE and MS-SSIM losses in (6) and (11). We use Resnet18 and its reverse architecture as the encoder and decoder for both the global and local IGD models in Fig. 3. When computing the accuracy of anomaly detection in MVTec AD, the threshold of the anomaly detection score $s(\mathbf{x})$ in (7) (to classify an image as anomalous) is estimated using the mean loss on the validation set, composed of 150 normal training images.

We also apply self-supervised contrastive learning (SSL) pre-training for both our models. Inspired by [22], we first apply rotation to augment the dataset by four folds (i.e.,

Pretrain	Method	MNIST	CIFAR10	FMNIST
Scratch	DAE [26]	0.8766	0.5358	-
	VAE [33]	0.9696	0.5833	-
	KDE [11]	0.8140	0.6100	-
	OCSVM [67]	0.9510	0.5860	-
	AnoGAN [66]	0.9127	0.6179	-
	DSVDD [62]	0.9480	0.6481	-
	OCGAN [54]	0.9750	0.6566	-
	PixelCNN [77]	0.6180	0.5510	-
	CapsNet _{pp} [39]	0.9770	0.6120	0.7650
	CapsNet _{trE} [39]	0.9250	0.5310	0.6790
	ADGAN [16]	0.9680	0.6340	-
	LSA [1]	0.9750	0.6410	0.8760
	MemAE [23]	0.9751	0.6088	-
	GradCon [35]	0.9730	0.6640	-
λ -VAE _u [17]	0.9820	0.7170	0.8730	
ULSLM [83]	0.9490	0.7360	-	
Ours	0.9869	0.7433	0.9201	
SSL	Rot-Net [22]	-	0.8160	0.9350
	Bergman et al. [6]	-	0.8820	0.9410
	Ours	-	0.9125	0.9441
Imagenet	CAVGA-D _u [78]	0.9860	0.7370	0.8850
	Student-Teacher [8]	0.9935	0.8196	-
	Ours	0.9927	0.8368	0.9357

Table 1. **Anomaly detection:** mean AUC results on MNIST, CIFAR10 and Fashion MNIST. The results are split into scratch without any pre-training, KD or pretrained with Imagenet and self-supervised learning (SSL). Bold numbers represent the best result (within 0.5%) for each data set, discriminated by scratch, SSL or Imagenet.

0, 90, 180, 270 degrees). Then we use the InfoNCE loss in [14] to contrast each data instance of the augmented dataset. In other words, our SSL can discriminate not only different image samples but also different rotation degrees. For this SSL pre-training, we use the SGD optimiser with a learning rate of 0.01, weight decay 10^{-1} , batch size of 32, and 2,000 epochs. Once we obtain the pre-trained encoder with SSL, we remove the MLP layer and attach a linear layer to the backbone with fixed parameters. Note that this SSL is trained from scratch. In contrast to the vanilla self-supervised learning [14] suggesting large batch size, we notice that a medium batch size yields significantly better performance for unsupervised anomaly detection. For the KD pre-training, we minimise the ℓ_2 norm between the 512-dimensional feature vector output from encoder and an intermediate layer of the ImageNet pre-trained ResNet18 [28] with the same 512-dimensional features. For this KD pre-training, we use the Adam optimiser with a learning rate of 0.0001, weight decay 10^{-5} , batch size of 64, and 50,000 iterations. Once we obtain the pre-trained encoder of KD, we fix the network parameters and attach a linear layer to reduce the dimensionality of the feature space to 128.

Metric	Method	Bottle	Hazelnut	Capsule	Metal Nut	Leather	Pill	Wood	Carpet	Tile	Grid	Cable	Transistor	Toothbrush	Screw	Zipper	Mean
Accuracy	AVID [64]	0.85	0.86	0.85	0.63	0.58	0.86	0.83	0.70	0.66	0.59	0.64	0.58	0.73	0.66	0.84	0.73
	AE _{SSIM} [9]	0.88	0.54	0.61	0.54	0.46	0.60	0.83	0.67	0.52	0.69	0.61	0.52	0.74	0.51	0.80	0.63
	DAE [26]	0.80	0.88	0.62	0.73	0.44	0.62	0.74	0.50	0.77	0.78	0.56	0.71	0.98	0.69	0.80	0.71
	AnoGAN [66]	0.69	0.50	0.58	0.50	0.52	0.62	0.68	0.49	0.51	0.51	0.53	0.67	0.57	0.35	0.59	0.55
	λ -VAE _u [17]	0.86	0.74	0.86	0.78	0.71	0.80	0.89	0.67	0.81	0.83	0.56	0.70	0.89	0.71	0.67	0.77
	LSA [1]	0.86	0.80	0.71	0.67	0.70	0.85	0.75	0.74	0.70	0.54	0.61	0.50	0.89	0.75	0.88	0.73
	CAVGA-D _u [78]	0.89	0.84	0.83	0.67	0.71	0.88	0.85	0.73	0.70	0.75	0.63	0.73	0.91	0.77	0.87	0.78
	CAVGA-R _u [78]	0.91	0.87	0.87	0.71	0.75	0.91	0.88	0.78	0.72	0.78	0.67	0.75	0.97	0.78	0.94	0.82
	Ours - KD	0.95	0.93	0.80	0.82	0.87	0.77	0.94	0.69	0.90	0.92	0.73	0.88	0.98	0.58	0.85	0.84
	Ours - SSL	0.95	0.93	0.81	0.82	0.90	0.74	0.89	0.71	0.94	0.90	0.79	0.85	0.98	0.67	0.88	0.85
AUC	AnoGAN [66]	0.800	0.259	0.442	0.284	0.451	0.711	0.567	0.337	0.401	0.871	0.477	0.692	0.439	0.100	0.715	0.503
	GANomaly [2]	0.794	0.874	0.721	0.694	0.808	0.671	0.920	0.821	0.720	0.743	0.711	0.808	0.700	1.000	0.744	0.782
	Skip-GANomaly [3]	0.937	0.906	0.718	0.790	0.908	0.758	0.919	0.795	0.850	0.657	0.674	0.814	0.689	1.000	0.663	0.805
	U-Net [61]	0.863	0.996	0.673	0.676	0.870	0.781	0.958	0.774	0.964	0.857	0.636	0.674	0.811	1.000	0.750	0.819
	DAGAN [72]	0.983	1.000	0.687	0.815	0.944	0.768	0.979	0.903	0.961	0.867	0.665	0.794	0.950	1.000	0.781	0.873
	Ours - KD	1.000	0.986	0.907	0.886	0.922	0.870	0.982	0.828	0.979	0.856	0.909	0.997	0.815	0.969	0.926	
	Ours - SSL	1.000	0.997	0.915	0.913	0.958	0.873	0.946	0.828	0.991	0.978	0.906	0.906	0.997	0.825	0.970	0.934

Table 2. **Anomaly detection:** mean accuracy and AUC on MVTec AD produced by the SOTA and our method. Best result in **red** and second best in **blue**.

4.3. Experiments on MNIST, Fashion MNIST and CIFAR10

Table 1 compares the unsupervised anomaly detection mean AUC results between our method and the current SOTA approaches in the field on MNIST, Fashion MNIST and CIFAR10. The rows labelled as ‘‘Scratch’’ show results of models without using any pre-training, and the ones with ‘‘SSL’’ display results from models using self-supervised learning method [6, 22]. The ones with ‘‘Imagenet’’ show results from models that use Imagenet information through pre-training [78] or KD [8]. Our ‘‘Scratch’’ IGD outperforms all current SOTA methods on all three datasets without any pre-training (see Tab. 1-Scratch), surpassing the previous SOTA λ -VAE_u [17] by 5% on FMNIST, 3% on CIFAR10 and 0.5% on MNIST in terms of the mean AUC. It is also interesting to note that our approach based on the proposed GSVDD obtains a 4.47% and 26.44% improvement on MNIST and CIFAR10, when compared with the original DSVDD [62], suggesting the effectiveness of our Gaussian SVDD.

Regarding pre-trained methods, in particular SSL approaches without using ImageNet information (see Tab. 1-SSL), our work achieves better results by a minimum 3% mean AUC on CIFAR10 and 0.3% mean AUC on FMNIST, compared with the current SOTA [6]. Considering Imagenet pre-trained methods, CAVGA-R_u [78] uses ImageNet [20] and Celeb-A [44] pre-trained ResNet18 models for the encoder and discriminator, respectively, while ours uses a smaller network to distill the information from the ImageNet pre-trained ResNet18. We show that our model achieves the SOTA results on all three datasets when comparing with CAVGA-R_u [78] and student-teacher network [8].

4.4. Experiments on MVTec AD

We report the results for both anomaly detection and localisation on MVTec AD, which contains real-world images of industry objects and textures containing different types of anomalies. We also show the results based on SSL and Imagenet KD pre-trained models. The mean accuracy of anomaly detection is displayed in Tab. 2 over all image classes, where our KD pre-trained model outperforms the previous SOTA methods CAVGA-D_u and CAVGA-R_u [78] by 6% and 2%, respectively, and our SSL pre-trained model outperforms their approach by 7% and 3%, respectively. With KD pre-training, our model achieves the best accuracy results in ten categories of the MVTec AD. The shallow generative baselines, such as DAE, AE-SSIM and AnoGAN yield sub-optimal results on MVTec AD. When compared with methods recently considered to be the MVTec AD SOTA, such as LSA [1] and λ -VAE_u [17], our approach shows more than 7% improvement. We also show the AUC anomaly detection results in Tab. 2, where our method, with SSL and ImageNet KD pre-training, surpasses all previous methods by at least 5.3%, and produces the best results in eleven categories. In Tables 2 and 2, we note that self-supervised learning approaches generally do not work well without a powerful anomaly detector for real-world anomaly images, such as the ones on MVTec AD [6, 22]. However, combining our IGD with the SSL pre-training, our model achieves the highest 93.4% mean AUC and 85% mean accuracy results and surpass the previous SOTA methods.

For anomaly localisation, we compare our method and the SOTA using the mean pixel-level AUC of all anomalous images in the testing set of MVTec AD – see Tab. 3. Notice that our method with KD and SSL are better than the previ-

Method	MVTec AD
DAE [26]	0.82
AE _{SSIM} [9]	0.87
AVID [64]	0.78
LSA [1]	0.79
λ -VAE _u [17]	0.86
AnoGAN [66]	0.74
ADVAE [40]	0.86
CAVGA-D _u [78]	0.85
CAVGA-R _u [78]	0.89
Ours - KD	0.91
Ours - SSL	0.93

Table 3. **Anomaly localisation:** mean pixel-level AUC results on the anomalous images of MVTEC AD. Best result in **red** and second best in **blue**.

ous SOTA CAVGA-R_u [78] by 2% and 4%, respectively. It is also important to note that our architecture is lighter than CAVGA-R_u given that it does not use an attention module and a visual discriminator. Fig. 1 shows anomaly localisation results on MVTEC AD images, where red regions in the heatmap indicate higher anomaly probability. From this results, we can see that our approach can localise anomalous regions of different sizes and structures from different object categories.

4.5. Experiments on Medical Datasets

To show that our method can generalise to other domains, we evaluate our approach on two public medical datasets - Hyper-Kvasir for polyp detection and LAG for glaucoma detection. As shown in Tab. 4, our SSL and KD based results achieve the best AUC results on both datasets. Our methods surpass the recent proposed CAVGA-R_u [78] on both datasets by a minimum 0.9% and maximum 3.8%. Also, our model performs better compared to the anomaly detector specifically designed for medical data, such as fanogan [65] and ADGAN [43]. The abnormalities in medical data (i.e., colon polyps, glaucoma) are significantly different than the synthetic data and MVTEC AD in terms of appearance and structural anomalies, suggesting that our model works in disparate domains.

Methods	Hyper-Kvasir	LAG
DAE [47]	0.705	0.651
CAM [92]	-	0.663
GBP [70]	-	0.787
SmoothGrad [69]	-	0.795
OCGAN [55]	0.813	0.737
F-anoGAN [65]	0.907	0.778
ADGAN [42]	0.913	0.752
CAVGA-R _u [78]	0.928	0.819
Ours - KD	0.931	0.838
Ours - SSL	0.937	0.857

Table 4. **Anomaly detection:** AUC results on two medical datasets: Hyper-Kvasir and LAG. Best result in **red** and second best in **blue**.

4.6. Ablation Study

To investigate the effectiveness of each component of our method, we show the mean AUC results of our method and its ablated variants on CIFAR10 in Tab. 5. The study starts with a model trained with the MS-SSIM reconstruction loss. This model achieves a mean AUC of 68.52%, which is higher than the 55.38% AUC from DAE model [26] that relies on MSE as the reconstruction loss (see Tab. 1). ImageNet KD pre-training (PT) then boosts the results by 4.6%. To show the importance of our proposed GSVDD, DSVDD improves MS-SSIM and KD by 6.4%, while GSVDD improves by 8.8%. Our proposed GSVDD provides larger improvement than KD pre-training. Adding ACAI interpolation (INTER) further improves the AUC by 1.7%. In addition to the results shown in Tab. 5, we also compare the results based on different reconstruction loss functions, namely: MS-SSIM, SSIM and MSE. MS-SSIM improves SSIM by 3.3% AUC and MSE by 4.9% AUC on CIFAR10.

MS-SSIM	PT	DSVDD	GSVDD	INTER	AUC - CIFAR10
✓					0.685
✓	✓				0.731
✓	✓	✓			0.795
✓	✓		✓		0.819
✓	✓		✓	✓	0.836

Table 5. Ablation study of our method on CIFAR10 using anomaly detection mean AUC (MS-SSIM: the backbone deep autoencoder with MS-SSIM loss, PT: knowledge distillation pre-training, DSVDD: Deep SVDD, GSVDD: our Gaussian SVDD, INTER: ACAI interpolation).

5. Conclusion

In this paper, we presented a new unsupervised anomaly detection and localisation method which learns a distribution of normal images that generalises well to all classes of normal images, a new criterion to detect and localise structural and non-structural multi-scale anomalies, and a new training that combines classification and reconstruction losses. Our learned distribution of normal images is based on the interpolated Gaussian descriptor (IGD) that provides a robust modelling of the normal image distribution with adversarially interpolated descriptors to regularise and facilitate the training of the proposed GSVDD. The proposed reconstruction loss can find structural and non-structural anomalies of varying sizes. The IGD and reconstruction losses are then jointly optimised to produce a global and a local model that achieves the best performance in the field on MNIST, CIFAR10, Fashion MNIST, MVTEC AD and two large scale medical datasets in terms of anomaly detection and localisation. We plan to study the use of GSVDD in the pixel-wise localisation of anomalies and the investigation of new self-supervised learning approaches specifically designed for anomaly detection.

References

- [1] Davide Abati, Angelo Porrello, Simone Calderara, and Rita Cucchiara. Latent space autoregression for novelty detection. In *Proceedings of the IEEE Conference on Computer Vision and Pattern Recognition*, pages 481–490, 2019. 2, 5, 6, 7, 8
- [2] Samet Akcay, Amir Atapour-Abarghouei, and Toby P Breckon. Ganomaly: Semi-supervised anomaly detection via adversarial training. In *Asian conference on computer vision*, pages 622–637. Springer, 2018. 3, 7
- [3] Samet Akçay, Amir Atapour-Abarghouei, and Toby P Breckon. Skip-ganomaly: Skip connected and adversarially trained encoder-decoder anomaly detection. In *2019 International Joint Conference on Neural Networks (IJCNN)*, pages 1–8. IEEE, 2019. 7
- [4] Arslan Basharat, Alexei Gritai, and Mubarak Shah. Learning object motion patterns for anomaly detection and improved object detection. In *2008 IEEE Conference on Computer Vision and Pattern Recognition*, pages 1–8. IEEE, 2008. 2
- [5] Christoph Baur, Benedikt Wiestler, Shadi Albarqouni, and Nassir Navab. Deep autoencoding models for unsupervised anomaly segmentation in brain mr images. In *International MICCAI Brainlesion Workshop*, pages 161–169. Springer, 2018. 3
- [6] Liron Bergman and Yedid Hoshen. Classification-based anomaly detection for general data. *arXiv preprint arXiv:2005.02359*, 2020. 1, 2, 5, 6, 7
- [7] Paul Bergmann, Michael Fauser, David Sattlegger, and Carsten Steger. Mvtec ad—a comprehensive real-world dataset for unsupervised anomaly detection. In *Proceedings of the IEEE Conference on Computer Vision and Pattern Recognition*, pages 9592–9600, 2019. 1, 2, 3, 5
- [8] Paul Bergmann, Michael Fauser, David Sattlegger, and Carsten Steger. Uninformed students: Student-teacher anomaly detection with discriminative latent embeddings. In *Proceedings of the IEEE/CVF Conference on Computer Vision and Pattern Recognition*, pages 4183–4192, 2020. 2, 3, 5, 6, 7
- [9] Paul Bergmann, Sindy Löwe, Michael Fauser, David Sattlegger, and Carsten Steger. Improving unsupervised defect segmentation by applying structural similarity to autoencoders. *arXiv preprint arXiv:1807.02011*, 2018. 2, 3, 4, 7, 8
- [10] David Berthelot, Colin Raffel, Aurko Roy, and Ian Goodfellow. Understanding and improving interpolation in autoencoders via an adversarial regularizer. *arXiv preprint arXiv:1807.07543*, 2018. 2, 3, 4
- [11] Christopher M Bishop. *Pattern recognition and machine learning*. springer, 2006. 6
- [12] Hanna Borgli and et al. Hyperkvasir, a comprehensive multi-class image and video dataset for gastrointestinal endoscopy. *Scientific Data*, 7(1):1–14, 2020. 2, 5, 6
- [13] Philippe Burlina, Neil Joshi, and I-Jeng Wang. Where’s wally now? deep generative and discriminative embeddings for novelty detection. In *Proceedings of the IEEE/CVF Conference on Computer Vision and Pattern Recognition (CVPR)*, June 2019. 2
- [14] Ting Chen, Simon Kornblith, Mohammad Norouzi, and Geoffrey Hinton. A simple framework for contrastive learning of visual representations. In *International conference on machine learning*, pages 1597–1607. PMLR, 2020. 5, 6
- [15] Kai-Wen Cheng, Yie-Tarng Chen, and Wen-Hsien Fang. Video anomaly detection and localization using hierarchical feature representation and gaussian process regression. In *Proceedings of the IEEE Conference on Computer Vision and Pattern Recognition (CVPR)*, June 2015. 2
- [16] Lucas Deecker, Robert Vandermeulen, Lukas Ruff, Stephan Mandt, and Marius Kloft. Image anomaly detection with generative adversarial networks. In *Joint european conference on machine learning and knowledge discovery in databases*, pages 3–17. Springer, 2018. 5, 6
- [17] David Dehaene, Oriël Frigo, Sébastien Combretelle, and Pierre Eline. Iterative energy-based projection on a normal data manifold for anomaly localization. *arXiv preprint arXiv:2002.03734*, 2020. 6, 7, 8
- [18] Allison Del Giorno, J Andrew Bagnell, and Martial Hebert. A discriminative framework for anomaly detection in large videos. In *European Conference on Computer Vision*, pages 334–349. Springer, 2016. 2
- [19] Arthur P Dempster, Nan M Laird, and Donald B Rubin. Maximum likelihood from incomplete data via the em algorithm. *Journal of the Royal Statistical Society: Series B (Methodological)*, 39(1):1–22, 1977. 3, 4
- [20] Jia Deng, Wei Dong, Richard Socher, Li-Jia Li, Kai Li, and Li Fei-Fei. Imagenet: A large-scale hierarchical image database. In *2009 IEEE conference on computer vision and pattern recognition*, pages 248–255. Ieee, 2009. 2, 7
- [21] Clément Godard, Oisín Mac Aodha, and Gabriel J Brostow. Unsupervised monocular depth estimation with left-right consistency. In *Proceedings of the IEEE Conference on Computer Vision and Pattern Recognition*, pages 270–279, 2017. 6
- [22] Izhak Golan and Ran El-Yaniv. Deep anomaly detection using geometric transformations. In *Advances in Neural Information Processing Systems*, pages 9758–9769, 2018. 1, 2, 5, 6, 7
- [23] Dong Gong, Lingqiao Liu, Vuong Le, Budhaditya Saha, Moussa Reda Mansour, Svetha Venkatesh, and Anton van den Hengel. Memorizing normality to detect anomaly: Memory-augmented deep autoencoder for unsupervised anomaly detection. In *Proceedings of the IEEE International Conference on Computer Vision*, pages 1705–1714, 2019. 1, 2, 4, 5, 6
- [24] Ian Goodfellow, Jean Pouget-Abadie, Mehdi Mirza, Bing Xu, David Warde-Farley, Sherjil Ozair, Aaron Courville, and Yoshua Bengio. Generative adversarial nets. In Z. Ghahramani, M. Welling, C. Cortes, N. D. Lawrence, and K. Q. Weinberger, editors, *Advances in Neural Information Processing Systems 27*, pages 2672–2680. Curran Associates, Inc., 2014. 4
- [25] Jianping Gou, Baosheng Yu, Stephen John Maybank, and Dacheng Tao. Knowledge distillation: A survey. *arXiv preprint arXiv:2006.05525*, 2020. 5
- [26] Raia Hadsell, Sumit Chopra, and Yann LeCun. Dimensionality reduction by learning an invariant mapping. In *2006 IEEE*

- Computer Society Conference on Computer Vision and Pattern Recognition (CVPR'06)*, volume 2, pages 1735–1742. IEEE, 2006. 6, 7, 8
- [27] Mahmudul Hasan, Jonghyun Choi, Jan Neumann, Amit K Roy-Chowdhury, and Larry S Davis. Learning temporal regularity in video sequences. In *Proceedings of the IEEE conference on computer vision and pattern recognition*, pages 733–742, 2016. 1
- [28] Kaiming He, Xiangyu Zhang, Shaoqing Ren, and Jian Sun. Deep residual learning for image recognition. In *Proceedings of the IEEE conference on computer vision and pattern recognition*, pages 770–778, 2016. 6
- [29] Ryota Hinami, Tao Mei, and Shin'ichi Satoh. Joint detection and recounting of abnormal events by learning deep generic knowledge. In *Proceedings of the IEEE International Conference on Computer Vision*, pages 3619–3627, 2017. 1
- [30] Geoffrey Hinton, Oriol Vinyals, and Jeff Dean. Distilling the knowledge in a neural network. *arXiv preprint arXiv:1503.02531*, 2015. 5
- [31] Radu Tudor Ionescu, Fahad Shahbaz Khan, Mariana-Iuliana Georgescu, and Ling Shao. Object-centric auto-encoders and dummy anomalies for abnormal event detection in video. In *Proceedings of the IEEE Conference on Computer Vision and Pattern Recognition*, pages 7842–7851, 2019. 2, 4
- [32] Diederik P Kingma and Jimmy Ba. Adam: A method for stochastic optimization. *arXiv preprint arXiv:1412.6980*, 2014. 6
- [33] Diederik P Kingma and Max Welling. Auto-encoding variational bayes. *arXiv preprint arXiv:1312.6114*, 2013. 6
- [34] Alex Krizhevsky, Vinod Nair, and Geoffrey Hinton. The cifar-10 dataset. *online: http://www.cs.toronto.edu/kriz/cifar.html*, 55, 2014. 1, 2, 5
- [35] Gukyeong Kwon, Mohit Prabhushankar, Dogancan Temel, and Ghassan AlRegib. Backpropagated gradient representations for anomaly detection, 2020. 6
- [36] Yann LeCun, Corinna Cortes, and CJ Burges. Mnist handwritten digit database. 2010. 2, 5
- [37] Liu Li et al. Attention based glaucoma detection: A large-scale database and cnn model. In *CVPR*, pages 10571–10580, 2019. 2, 5, 6
- [38] Liu Li, Mai Xu, Xiaofei Wang, Lai Jiang, and Hanruo Liu. Attention based glaucoma detection: A large-scale database and cnn model. In *Proceedings of the IEEE/CVF Conference on Computer Vision and Pattern Recognition (CVPR)*, June 2019. 3
- [39] Xiaoyan Li, Iluju Kiringa, Tet Yeap, Xiaodan Zhu, and Yifeng Li. Exploring deep anomaly detection methods based on capsule net. In *Canadian Conference on Artificial Intelligence*, pages 375–387. Springer, 2020. 6
- [40] Wenqian Liu, Runze Li, Meng Zheng, Srikrishna Karanam, Ziyang Wu, Bir Bhanu, Richard J Radke, and Octavia Camps. Towards visually explaining variational autoencoders. In *Proceedings of the IEEE/CVF Conference on Computer Vision and Pattern Recognition*, pages 8642–8651, 2020. 8
- [41] Wen Liu, Weixin Luo, Dongze Lian, and Shenghua Gao. Future frame prediction for anomaly detection—a new baseline. In *Proceedings of the IEEE Conference on Computer Vision and Pattern Recognition*, pages 6536–6545, 2018. 1, 2
- [42] Y. Liu, Y. Tian, G. Maicas, L. Z. Cheng Tao Pu, R. Singh, J. W. Verjans, and G. Carneiro. Photoshopping colonoscopy video frames. In *2020 IEEE 17th International Symposium on Biomedical Imaging (ISBI)*, pages 1–5, 2020. 8
- [43] Yuyuan Liu, Yu Tian, Gabriel Maicas, Leonardo ZCT Pu, Rajvinder Singh, Johan W Verjans, and Gustavo Carneiro. Photoshopping colonoscopy video frames. *arXiv preprint arXiv:1910.10345*, 2019. 3, 8
- [44] Ziwei Liu, Ping Luo, Xiaogang Wang, and Xiaoou Tang. Large-scale celebfaces attributes (celeba) dataset. 2, 7
- [45] Weixin Luo, Wen Liu, and Shenghua Gao. A revisit of sparse coding based anomaly detection in stacked rnn framework. In *Proceedings of the IEEE International Conference on Computer Vision*, pages 341–349, 2017. 1
- [46] Amir Markovitz, Gilad Sharir, Itamar Friedman, Lih Zelnik-Manor, and Shai Avidan. Graph embedded pose clustering for anomaly detection. In *IEEE/CVF Conference on Computer Vision and Pattern Recognition (CVPR)*, June 2020. 2
- [47] Jonathan Masci and et al. Stacked convolutional auto-encoders for hierarchical feature extraction. In *International Conference on Artificial Neural Networks*, pages 52–59. Springer, 2011. 8
- [48] Gérard Medioni, Isaac Cohen, François Brémond, Somboon Hongeng, and Ramakant Nevatia. Event detection and analysis from video streams. *IEEE Transactions on pattern analysis and machine intelligence*, 23(8):873–889, 2001. 2
- [49] Romero Morais, Vuong Le, Truyen Tran, Budhaditya Saha, Moussa Mansour, and Svetha Venkatesh. Learning regularity in skeleton trajectories for anomaly detection in videos. In *Proceedings of the IEEE Conference on Computer Vision and Pattern Recognition*, pages 11996–12004, 2019. 2
- [50] Trong-Nguyen Nguyen and Jean Meunier. Anomaly detection in video sequence with appearance-motion correspondence. In *Proceedings of the IEEE International Conference on Computer Vision*, pages 1273–1283, 2019. 2
- [51] Guansong Pang, Chunhua Shen, Longbing Cao, and Anton van den Hengel. Deep learning for anomaly detection: A review. *arXiv preprint arXiv:2007.02500*, 2020. 2
- [52] Hyunjong Park, Jongyoun Noh, and Bumsu Ham. Learning memory-guided normality for anomaly detection. In *IEEE/CVF Conference on Computer Vision and Pattern Recognition (CVPR)*, June 2020. 2
- [53] Adam Paszke, Sam Gross, Francisco Massa, Adam Lerer, James Bradbury, Gregory Chanan, Trevor Killeen, Zeming Lin, Natalia Gimelshein, Luca Antiga, Alban Desmaison, Andreas Kopf, Edward Yang, Zachary DeVito, Martin Raison, Alykhan Tejani, Sasank Chilamkurthy, Benoit Steiner, Lu Fang, Junjie Bai, and Soumith Chintala. Pytorch: An imperative style, high-performance deep learning library. In H. Wallach, H. Larochelle, A. Beygelzimer, F. d'Alché-Buc, E. Fox, and R. Garnett, editors, *Advances in Neural Information Processing Systems 32*, pages 8024–8035. Curran Associates, Inc., 2019. 6
- [54] Pramuditha Perera, Ramesh Nallapati, and Bing Xiang. Ocgan: One-class novelty detection using gans with constrained latent representations. In *Proceedings of the IEEE Conference on Computer Vision and Pattern Recognition*, pages 2898–2906, 2019. 1, 2, 5, 6

- [55] Pramuditha Perera, Ramesh Nallapati, and Bing Xiang. Ocgan: One-class novelty detection using gans with constrained latent representations. In *Proceedings of the IEEE Conference on Computer Vision and Pattern Recognition*, pages 2898–2906, 2019. 8
- [56] Gunnar Rätsch, Bernhard Schölkopf, Sebastian Mika, and Klaus-Robert Müller. *SVM and boosting: One class*. GMD-Forschungszentrum Informationstechnik, 2000. 1
- [57] Mahdyar Ravanbakhsh, Moin Nabi, Hossein Mousavi, Enver Sangineto, and Nicu Sebe. Plug-and-play cnn for crowd motion analysis: An application in abnormal event detection. In *2018 IEEE Winter Conference on Applications of Computer Vision (WACV)*, pages 1689–1698. IEEE, 2018. 1
- [58] Mahdyar Ravanbakhsh, Moin Nabi, Enver Sangineto, Lucio Marcenaro, Carlo Regazzoni, and Nicu Sebe. Abnormal event detection in videos using generative adversarial nets. In *2017 IEEE International Conference on Image Processing (ICIP)*, pages 1577–1581. IEEE, 2017. 1
- [59] Mahdyar Ravanbakhsh, Enver Sangineto, Moin Nabi, and Nicu Sebe. Training adversarial discriminators for cross-channel abnormal event detection in crowds. In *2019 IEEE Winter Conference on Applications of Computer Vision (WACV)*, pages 1896–1904. IEEE, 2019. 3
- [60] Huamin Ren, Weifeng Liu, Søren Ingvar Olsen, Sergio Escalera, and Thomas B Moeslund. Unsupervised behavior-specific dictionary learning for abnormal event detection. In *BMVC*, pages 28–1, 2015. 2, 4
- [61] Olaf Ronneberger, Philipp Fischer, and Thomas Brox. U-net: Convolutional networks for biomedical image segmentation. In *International Conference on Medical image computing and computer-assisted intervention*, pages 234–241. Springer, 2015. 7
- [62] Lukas Ruff, Robert Vandermeulen, Nico Goernitz, Lucas Deecke, Shoaib Ahmed Siddiqui, Alexander Binder, Emmanuel Müller, and Marius Kloft. Deep one-class classification. In *International conference on machine learning*, pages 4393–4402, 2018. 1, 2, 4, 5, 6, 7
- [63] Mohammad Sabokrou, Mohsen Fayyaz, Mahmood Fathy, and Reinhard Klette. Deep-cascade: Cascading 3d deep neural networks for fast anomaly detection and localization in crowded scenes. *IEEE Transactions on Image Processing*, 26(4):1992–2004, 2017. 2
- [64] Mohammad Sabokrou, Mohammad Khaloeei, Mahmood Fathy, and Ehsan Adeli. Adversarially learned one-class classifier for novelty detection. In *Proceedings of the IEEE Conference on Computer Vision and Pattern Recognition*, pages 3379–3388, 2018. 2, 7, 8
- [65] Thomas Schlegl, Philipp Seeböck, Sebastian M Waldstein, Georg Langs, and Ursula Schmidt-Erfurth. f-anogan: Fast unsupervised anomaly detection with generative adversarial networks. *Medical image analysis*, 54:30–44, 2019. 1, 3, 8
- [66] Thomas Schlegl, Philipp Seeböck, Sebastian M Waldstein, Ursula Schmidt-Erfurth, and Georg Langs. Unsupervised anomaly detection with generative adversarial networks to guide marker discovery. In *International conference on information processing in medical imaging*, pages 146–157. Springer, 2017. 1, 3, 6, 7, 8
- [67] Bernhard Schölkopf, John C Platt, John Shawe-Taylor, Alex J Smola, and Robert C Williamson. Estimating the support of a high-dimensional distribution. *Neural computation*, 13(7):1443–1471, 2001. 6
- [68] Bernhard Schölkopf, Robert C Williamson, Alex J Smola, John Shawe-Taylor, and John C Platt. Support vector method for novelty detection. In *Advances in neural information processing systems*, pages 582–588, 2000. 2
- [69] Daniel Smilkov, Nikhil Thorat, Been Kim, Fernanda Viégas, and Martin Wattenberg. Smoothgrad: removing noise by adding noise. *arXiv preprint arXiv:1706.03825*, 2017. 8
- [70] Jost Tobias Springenberg, Alexey Dosovitskiy, Thomas Brox, and Martin Riedmiller. Striving for simplicity: The all convolutional net. *arXiv preprint arXiv:1412.6806*, 2014. 8
- [71] Waqas Sultani, Chen Chen, and Mubarak Shah. Real-world anomaly detection in surveillance videos. In *Proceedings of the IEEE Conference on Computer Vision and Pattern Recognition*, pages 6479–6488, 2018. 2
- [72] Ta-Wei Tang, Wei-Han Kuo, Jauh-Hsiang Lan, Chien-Fang Ding, Hakiem Hsu, and Hong-Tsu Young. Anomaly detection neural network with dual auto-encoders gan and its industrial inspection applications. *Sensors*, 20(12):3336, 2020. 7
- [73] David MJ Tax and Robert PW Duin. Support vector data description. *Machine learning*, 54(1):45–66, 2004. 2, 3
- [74] Yu Tian, Gabriel Maicas, Leonardo Zorron Cheng Tao Pu, Rajvinder Singh, Johan W Verjans, and Gustavo Carneiro. Few-shot anomaly detection for polyp frames from colonoscopy. In *Medical Image Computing and Computer Assisted Intervention—MICCAI 2020: 23rd International Conference, Lima, Peru, October 4–8, 2020, Proceedings, Part VI 23*, pages 274–284. Springer, 2020. 1
- [75] Yu Tian, Leonardo ZCT Pu, Rajvinder Singh, Alastair D Burt, and Gustavo Carneiro. One-stage five-class polyp detection and classification. In *2019 IEEE 16th International Symposium on Biomedical Imaging (ISBI 2019)*, pages 70–73. IEEE, 2019. 2
- [76] Yu Tian, Leonardo Zorron Cheng Tao Pu, Yuyuan Liu, Gabriel Maicas, Johan W Verjans, Alastair D Burt, Seon Ho Shin, Rajvinder Singh, and Gustavo Carneiro. Detecting, localising and classifying polyps from colonoscopy videos using deep learning. *arXiv preprint arXiv:2101.03285*. 1
- [77] Aaron Van den Oord, Nal Kalchbrenner, Lasse Espeholt, Oriol Vinyals, Alex Graves, et al. Conditional image generation with pixelcnn decoders. In *Advances in neural information processing systems*, pages 4790–4798, 2016. 6
- [78] Shashanka Venkataraman, Kuan-Chuan Peng, Rajat Vikram Singh, and Abhijit Mahalanobis. Attention guided anomaly detection and localization in images. *arXiv preprint arXiv:1911.08616*, 2019. 1, 2, 3, 4, 5, 6, 7, 8
- [79] Jue Wang and Anoop Cherian. Gods: Generalized one-class discriminative subspaces for anomaly detection. In *Proceedings of the IEEE International Conference on Computer Vision*, pages 8201–8211, 2019. 2
- [80] Jiang Wang, Yang Song, Thomas Leung, Chuck Rosenberg, Jingbin Wang, James Philbin, Bo Chen, and Ying Wu. Learning fine-grained image similarity with deep ranking. In *Pro-*

- ceedings of the IEEE Conference on Computer Vision and Pattern Recognition*, pages 1386–1393, 2014. 2
- [81] Zhou Wang, Alan C Bovik, Hamid R Sheikh, and Eero P Simoncelli. Image quality assessment: from error visibility to structural similarity. *IEEE transactions on image processing*, 13(4):600–612, 2004. 2, 4
- [82] Zhou Wang, Eero P Simoncelli, and Alan C Bovik. Multi-scale structural similarity for image quality assessment. In *The Thirty-Seventh Asilomar Conference on Signals, Systems & Computers, 2003*, volume 2, pages 1398–1402. Ieee, 2003. 2, 4
- [83] Lior Wolf, Sagie Benaim, and Tomer Galanti. Unsupervised learning of the set of local maxima. *arXiv preprint arXiv:2001.05026*, 2020. 6
- [84] Peng Wu, jing Liu, Yujia Shi, Yujia Sun, Fangtao Shao, Zhaoyang Wu, and Zhiwei Yang. Not only look, but also listen: Learning multimodal violence detection under weak supervision. In *European Conference on Computer Vision (ECCV)*, 2020. 2
- [85] Han Xiao, Kashif Rasul, and Roland Vollgraf. Fashion-mnist: a novel image dataset for benchmarking machine learning algorithms, 2017. 2, 5
- [86] Dan Xu, Elisa Ricci, Yan Yan, Jingkuan Song, and Nicu Sebe. Learning deep representations of appearance and motion for anomalous event detection. *arXiv preprint arXiv:1510.01553*, 2015. 2, 4
- [87] Hongyi Zhang, Moustapha Cisse, Yann N Dauphin, and David Lopez-Paz. mixup: Beyond empirical risk minimization. *arXiv preprint arXiv:1710.09412*, 2017. 4
- [88] Tianzhu Zhang, Hanqing Lu, and Stan Z Li. Learning semantic scene models by object classification and trajectory clustering. In *2009 IEEE conference on computer vision and pattern recognition*, pages 1940–1947. IEEE, 2009. 2
- [89] Ying Zhang, Huchuan Lu, Lihe Zhang, Xiang Ruan, and Shun Sakai. Video anomaly detection based on locality sensitive hashing filters. *Pattern Recognition*, 59:302–311, 2016. 1
- [90] Hang Zhao, Orazio Gallo, Iuri Frosio, and Jan Kautz. Loss functions for image restoration with neural networks. *IEEE Transactions on computational imaging*, 3(1):47–57, 2016. 2, 6
- [91] Jia-Xing Zhong, Nannan Li, Weijie Kong, Shan Liu, Thomas H Li, and Ge Li. Graph convolutional label noise cleaner: Train a plug-and-play action classifier for anomaly detection. In *Proceedings of the IEEE Conference on Computer Vision and Pattern Recognition*, pages 1237–1246, 2019. 2
- [92] Bolei Zhou, Aditya Khosla, Agata Lapedriza, Aude Oliva, and Antonio Torralba. Learning deep features for discriminative localization. In *Proceedings of the IEEE conference on computer vision and pattern recognition*, pages 2921–2929, 2016. 8
- [93] Kang Zhou, Yuting Xiao, Jianlong Yang, Jun Cheng, Wen Liu, Weixin Luo, Zaiwang Gu, Jiang Liu, and Shenghua Gao. Encoding structure-texture relation with p-net for anomaly detection in retinal images. *arXiv preprint arXiv:2008.03632*, 2020. 2
- [94] Bo Zong, Qi Song, Martin Renqiang Min, Wei Cheng, Cristian Lumezanu, Daeki Cho, and Haifeng Chen. Deep autoencoding gaussian mixture model for unsupervised anomaly detection. In *International Conference on Learning Representations*, 2018. 2